Carbohydrate Polymer Technologies and Applications 6 (2023) 100405

Contents lists available at ScienceDirect

Carbohydrate Polymer Technologies and Applications

journal homepage: www.sciencedirect.com/journal/carbohydrate-polymer-technologies-and-applications

Alginate microgels encapsulation strategy of silver nanoparticles active against *Candida albicans*

Mélanie Marquis [a,b,*], Dafne Musino [a], Valentin Gemin [a], Laetitia Kolypczuk [c], Delphine Passerini [c], Isabelle Capron [a,*]

[a] INRAE, UR1268 Biopolymers Interactions and Assemblies, 44300 Nantes, France
[b] Oniris, INRAE, UMR0703 Physiopathologie Animale et BioThérapie du muscle et du système nerveux, 44307 Nantes, France
[c] Ifremer, MASAE Microbiologie Aliment Santé Environnement, 44000 Nantes, France

ARTICLE INFO

Keywords:
Cellulose nanocrystal (CNC)
Chitin nanocrystal (ChiNC)
Hybrid
Microfluidic
Hydrogel
Antimicrobial activities

ABSTRACT

Nanoparticles (NPs), offering high specific surface, are considered as the best potential anti-microbial agents for a wide range of medical nanotechnology. Among them, silver NPs (AgNPs) allow high biocidal activity. A design of ecological capsules is proposed where AgNPs of 22 nm in diameter are grafted on the surface of biobased nanocrystals obtained from cellulose (CNC) and chitin (ChiNC). These silver nanohybrids are dispersed in calcium-alginate microgels of 45–50 μm in diameter using microfluidic tools. Such double level of immobilization of AgNPs leads to highly stable carriers, prolongs shelf life and raises bioactivity, with a precise control of well dispersed AgNPs as determined by scanning transmission electron microscopy, UV-Vis spectroscopy and atomic absorption spectroscopy. Preliminary tests for antimicrobial activities of these new microgels have shown a significant inhibitory effect on *Candida albicans*, the most common fungal pathogen, responsible for thrush and vaginal yeast infections, for very low levels of silver.

1. Introduction

In the recent fast development of medical nanotechnology, nanoparticles (NPs) are considered as new potential anti-microbial agents, notably against many bacteria, viruses, fungi, and protozoan species (Cai et al., 2021; Dakal et al., 2016; Ernest Ravindran et al., 2020; Gómez-Garzón et al., 2021a; Hendiger et al., 2020; Nikolov et al., 2021; Rahman et al., 2019). Particularly, silver NPs are known to show antibacterial activity. The adhesion of AgNPs onto the surface of the cell membrane of microorganisms leads to membrane alteration and disruption of cell activity causing damage to intracellular organelles and biomolecules. Moreover, AgNPs increase the amount of reactive oxygen species (ROS) that modulate signal transduction pathways causing cell death (Dakal et al., 2016; Hendiger et al., 2020; Neves et al., 2021). Studies have shown that the antimicrobial action of AgNPs is intensely dependent on their shape, size, concentration and colloidal state (Dakal et al., 2016). Notably, it was shown that the nanometric size of AgNPs leading to a high specific surface area was the main factor affecting biocidal activity, unlike their internal structure (Musino et al., 2021). Their aggregation can also have a negative impact on their antibacterial efficiency. The hybridization of metal NPs on larger supports limits this phenomenon and increases the specific surface area resulting in a better efficiency to antibacterial effect at lower concentration (Zhou et al., 2013). Recently, AgNPs were stabilized with polyvinylalcohol (PVA) using droplet-based microfluidic reactors resulting in suspension of hybrids of 17 nm with antibacterial activity (Bashir et al., 2022).

To open up the green route, the nano-biotechnology uses NPs naturally biosynthesized (Gómez-Garzón et al., 2021a;Thiruvengadam & Pandidurai, 2014; Ullah et al., 2018). Biopolymers, with chelating ability, are good stabilizers of silver through polymer-metal interactions (Rojas et al., 2023). The biodegradability of substrates is also useful for antibacterial treatment applications. Thereby, cellulose nanocrystals (CNCs) obtained from plants (Klemm et al., 2011), and chitin nanocrystals (ChiNCs) obtained from arthropod exoskeleton or fungi and yeast cell walls (Perrin et al., 2014) are safe for the environment, sustainable and globally available in large quantities. CNCs and ChiNCs represent attractive biopolymeric templates and stabilizers for the synthesis of AgNPs, and allow the production of hybrid nanomaterials dispersible in water valuable for a large range of applications. Recently, AgNPs between 16 and 18 nm were grafted onto the surface of CNCs

* Corresponding author at: Oniris, INRAE, UMR0703 Physiopathologie Animale et BioThérapie du muscle et du système nerveux, 44307 Nantes, France.
E-mail address: melanie.marquis@inrae.fr (M. Marquis).

https://doi.org/10.1016/j.carpta.2023.100405

Available online 10 December 2023

after reduction of $AgNO_3$ salt by $NaBH_4$ using a simple preparation in aqueous medium. Hydroxyl groups on the CNC surface were identified as nucleation points for AgNPs (Musino et al., 2020; 2021). With this grafting method on cellulose substrate, amount of individual AgNP was controlled. To date, this hybridization method was only demonstrated on a cellulose substrate. The use of other bio-based substrates to develop new ecological hybrids is required to reach a wider range of applications.

The development of alternative delivery systems involving metal NPs is gaining much attention due to their significant potent antimicrobial therapeutic activity (Aisida et al., 2020; Ou et al., 2020). Various methods using electrospinning (Ferashteh et al., 2019) or photo-polymerization batch methods (Leawhiran et al., 2014; Ou et al., 2020) were developped based on functional synthetic polymers to obtain medical carriers such as wound dressing or injectable matrix. These encapsulation techniques improved the release and targeting ability of metal NPs. In this way, Monerris et *al.* developed a method to encapsulate AgNPs inside swollen hydrogel based on N-isopropylacrylamide and derivatives, thanks to *in-situ* photoreduction of Ag^+ ions. This original method avoids the dispersion of AgNPs and regulates Ag^+ ions release rate (Monerris et al., 2017). Various biocompatible synthetic materials with a diameter and a thickness around 1 cm and 200 μm respectively can be thus produced. However, the lack of control of morphological and biodegradability characteristics limits the use of these materials for medical applications such as local injection in specific tissues. Biodegradable and biocompatible materials from natural sources have emerged as materials intented to interface with biological systems in the treatment of infectious diseases (Muñoz-Bonilla et al., 2019; Williams, 2009). Various gelling polysaccharides from natural sources, such as alginate (Matalanis et al., 2011), chitosan (Dang et al., 2016), or pectine (Marquis et al., 2014) form networks physically connected through hydrogen-bonds or electrostatic interactions. In this way, droplet-based microfluidics were used to encapsulate AgNPs in uniform and monodisperse chitosan microparticles with controlled size between 294 μm and 630 μm (Yang et al., 2016). The simple and bio-friendly approach offered solid chitosan microparticles impregnated with AgNPs exhibiting antimicrobial activities. The combination of chitosan with other materials, e.g. natural polymers, is usually used to overcome breakable hydrogels that are less suitable for delivery system applications (Seidi et al., 2021; Shoueir et al., 2021).

The immobilization of synthetic AgNPs nanowires using vanadium oxide as the reductant and stabilizer was recently developed. The synthetic nanowires were then loaded into alginate microfibers prepared *via* electrospinning to limit infections by microorganisms and reduce inflammatory reaction in wound healing (Huang et al., 2022). The present work proposes to apply this approach to produce bio-based silver nanohybrids compatible to local treatment injection applications. To enhance properties and activities, biopolymer sources will be mixed. Whereas cellulose or chitin nanocrystals offer bio-based substrate for the AgNPs synthesis, alginate is one of the most used natural polymers in biomedical field due to its biocompatibility and its ability to form a strong hydrogel network (Cinel et al., 2021; Mancini et al., 1999; Markert et al., 2013). This work focuses on (1) the expansion of bio-based hybridization of Ag^+ using ChiNC as biodegradable and sustainable substrate on which 8 wt% of AgNP are grafted onto surface only, then (2) the encapsulation of bio-based silver nanohybrids in alginate-based microhydrogels to better control the size and content of AgNPs and to avoid their aggregation. CNC/AgNPs and ChiNC/AgNPs nanohybrids will be encapsulated in alginate microgels of approximately 50 μm in diameter *via* microfluidic methods, to improve and control the localized distribution of NPs by limiting the diffusion in the host receiving local injection of antibiotic treatments.

2. Materials & methods

2.1. Materials

Cellulose nanocrystals (CNCs) were purchased from CelluForce (product num. 2015–009, Canada). CNCs were extracted from bleached Kraft pulp performing an acid hydrolysis procedure and then neutralized to sodium form and spray-dried (length = 183 ± 88 nm; cross-section = 6 ± 2 nm; aspect ratio = 31) (Reid et al., 2017). Chitin nanocrsystals (ChiNCs) were extracted from commercial shrimp shell powder (Sigma-Aldrich, France) by acid hydrolysis according to the experimental procedure developed by Perrin et al. (2014). Briefly, an amount of 4 g of shrimp shell powder were dispersed in 80 mL of boiling 3 N HCl solution and put under stirring for 90 min. The resulting suspension was neutralized and purified by filtration (1.2 μm pore size cellulose nitrate membranes, Millipore, USA) and finally suspended in water. Then, a dialysis step was performed against ultrapure water for 10 days and the final ChiNC aqueous suspension was at pH 5.5 with a ChiNC concentration of 15 g/L. The ChiNCs had a length of 150–250 nm and a width of about 20 nm (Jiménez-Saelices et al., 2020). Silver nitrate ($AgNO_3 \geq 99$ %), sodium borohydride ($NaBH_4 \geq 96$ %), 2,2,6,6-Tetramethylpiperidine 1-oxyl (TEMPO: 98.8 %), sodium bromide (NaBr: 99 %), sodium hypochlorite solution (NaClO: 10 % RT) were purchased from Sigma-Aldrich and used without further purification. Alginate (Mw = 151 550 g/mol, Ip = 2.11) was obtained from FMC biopolymer (U.S.A). Freeze-dried $CaCO_3$ powder was provided by Mikhart Provençale S.A. Sunflower seed oil was purchased from Fluka. Sodium chloride (NaCl), calcium chloride ($CaCl_2$), Span 80 and acetic acid were purchased from Sigma-Aldrich. For all the aqueous suspensions, ultra-pure water was used.

2.2. Surface-modification of ChiNCs via TEMPO-mediated oxidation (TChiNCs)

To perform the surface carboxylation of ChiNCs, TEMPO-mediated oxidation was performed using an experimental method proposed by Musino et al. (2021) which was adapted from the work of Araki & Hida (2018). Oxidation of CNC using 2,2,6,6-tetramethylpyperidine-1-oxyl (TEMPO), inducing carboxyl groups onto the surface, appeared to be an excellent strategy as it improved the hydroxyl groups accessibility. A volume of 100 mL of ChiNCs suspension (2 g/L) was mixed with 0.25 g of NaBr and 0.05 g of TEMPO. Then, a volume 2.5 mL of NaClO was dropwise added to start the carboxylation leading to a pH increase. The suspension was stirred at room temperature for 24 h keeping the pH at 10.3 by the controlled injection of 0.1 M NaOH solution using an automatic titrator (Metrohm 901 Titrando, France). It was then centrifuged twice (10 min; 10,000 g), dispersed in ultra-pure water to obtain a final concentration of 15 g/L and finally homogenized by ultrasound (amplitude = 10; 5 min). The final suspension was dialyzed against ultra-pure water for one week (dialysis bath volume to sample volume = 10:1) in order to completely remove the residual contaminants.

2.3. Synthesis of CNC/AgNP, ChiNC/AgNP and TChiNC/AgNP hybrid suspensions

To synthetize CNC/AgNP, ChiNC/AgNP and TChiNC/AgNP hybrid suspension where AgNPs are nucleated and well-dispersed on the bio-based support, the experimental method proposed in one of previous works was used (Musino et al., 2020; 2021). Briefly, a volume of 9.8 mL of CNC, ChiNC or TChiNC aqueous suspension (15 g/L) were mixed at room temperature for 1 min with an amount of 2 mL of $AgNO_3$ aqueous solution (0.05 M). A volume of 1.5 mL freshly prepared $NaBH_4$ aqueous solution (20 mL, $AgNO_3/NaBH_4$ molar ratio equal to 1.5) was added to the suspension in order to induce the reduction of Ag^+ ions thus forming AgNPs (i.e., color sample from translucent to yellow). During the preparation, all the samples were covered with aluminum foil to avoid

AgNP oxidation and mixed at room temperature for 24 h. Finally, the CNC/AgNP, ChiNC/AgNP and TChiNC/AgNP hybrid suspensions were dialyzed against water for 24 h (dialysis bath volume to sample volume = 10:1).

2.4. Characterization of CNC/AgNP, ChiNC/AgNP and TChiNC/AgNP hybrid suspensions

2.4.1. Scanning transmission electron microscopy (STEM)

A Quattro S field emission gun scanning microscope (Thermo Fisher Scientific, USA) equipped with a STEM detector was used for the acquisition of STEM Images, working at 10 kV. Firstly, the samples were diluted with ultra-pure water at 0.5 g/L in CNC, ChiNC or TChiNC content. Then, 10 μL were deposited on glow-discharged carbon coated grids (200 meshes, Delta Microscopies, France) for two minutes. The excess was then removed using Whatman filter paper and the grids were dried in air for 12 h and finally coated with a 0.5 nm platinum layer using an ion-sputter coater (LEICA AM ACE600, Germany). The acquired STEM images were analyzed using ImageJ software. The AgNP size distributions were obtained considering the mean AgNP Feret's diameter (i.e., the largest distance between two tangents to the contour of the measured particle) considering the largest possible number of AgNPs (at least 100, depending on the sample).

2.4.2. UV-Vis spectroscopy

A Mettler-Toledo UV7 spectrophotometer (Columbus, OH, USA) equipped with a 10 mm quartz cell was used to record light-visible spectra of the hybrid suspensions in the 300–900 nm range. The suspensions were diluted (1:10) and ultra-pure water was used as a blank reference.

2.4.3. Atomic absorption spectroscopy (AAS)

The effective AgNP content in each hybrid suspension was estimated by Atomic Absorption Spectroscopy (ICE 3300 AAS, Thermo Fisher, USA). A volume of 0.5 mL of hybrid was mixed with H_2O/aqua regia mixture (i.e., 40 mL, 30 % v aqua regia; HCl/HNO_3: 3/1) for 24 h and then analyzed. A calibration curve was defined using a silver standard solution (1000 μg/mL, Chem-Lab NV) at various concentrations, from 0.25 to 10 ppm. For each sample, two independent measurements were performed and the final AgNP content was expressed in mg of AgNP per g of sample.

2.4.4. X-ray powder diffraction

For each sample, an XRD diffractogram was recorded using a Bruker D8 Discover diffractometer. A Cu-Kα1 radiation (Cu Kα1, 1.5405 Å) was produced in a sealed tube at 40 kV and a 40 mA was selected and parallelized using a Gobël mirror parallel optics system and collimated to produce a 500 mm beam diameter. The acquisition time was fixed at 10 min in the 3°−70° 2θ range.

2.5. Preparation of alginate hydrogel microparticles containing NPs using microfluidic tools

2.5.1. Production of the microfluidic flow-focusing device

The microfluidic device, comprising a Flow Focusing Device (FFD) junction and a second one for the continuous phase, was prepared following a method previously optimized (Marquis et al., 2016). Briefly, the design of the device was drawn using Adobe Illustrator software to obtain a photomask printed by high resolution printing. Dimensions of the channels are shown on Figure S2. Then the mold was made using photolithography techniques with a UV LED masker (UV-KUB 2, Kloé, France) to obtain SU-8 2100 (CTS, France) positive relief structures, of 130 μm in height, on silicone wafers. Finally, the microfluidic flow-focusing device was fabricated by soft lithography technique using poly(dimethylsiloxane) (PDMS) (RTV 615, Elecoproduit, France). Two PDMS polymer / crosslinker mixtures (10 % and 5 % crosslinker) were poured on the mold and in a Petri dish, respectively. After degassing, the PDMS was cured 30 min at 70 °C. The curde PDMS (10 % crosslinker) was cut and peeled off the mold and access holes were punched. Then, the PDMS layer (10 % crosslinker) was cleaned and placed in contact with the thin PDMS layer (5 % crosslinker) to generate the microchip by gradient diffusion of the cross-linker diffusion during curing at 70 °C for 24 h. The outlet at the end of the PDMS microdevice was parallel to the central channel and a polytetrafluoroethylene (PTFE) tube (inner diameter, 0.3 mm; outer diameter, 0.76 mm; length, 20 cm) was directly inserted into a PDMS short exit channel (depth, 130 μm; width, 400 μm; length, 5 mm).

2.5.2. Preparation of calcium-alginate microgels containing nanohybrids

The generation of Ca-alginate microgels containing nanohybrids was optimized by droplet-based microfluidic tools following methods detailed in previous works (Marquis et al., 2012, 2016). The dispersed phase (Qd) was composed of an aqueous solution of alginate at 1.0 wt% and $CaCO_3$ at 0.2 wt% with the latter being the cross-linking agent in its inative form. From this aqueous solution, three solutions containing nanometerial suspensions were prepared with CNC at 0.5 wt%, CNC/Ag at 0.5 wt% or TChiNC/Ag at 0.5 wt%. $CaCO_3$ particles and nanohybrids contained in the aqueous solution were gently dispersed using vortex mixing. The two continuous phases were composed of sunflower seed oil and 0.5 wt% of Span 80. The second continuous phase (Qc2) differs from the first one (Qc1) in added acetic acid at 0.5 wt% which acts as the cross-linking activator. Flow rates of 5 μL/min for the aqueous dispersed phase (Qd) and 90 μL/min for continuous phases (Qc1 and Qc2) were applied, using digitally controlled syringe pumps (Harvard Apparatus PHD 2000, France), to generate droplets and their gelation. Finally, microgels containing nanohybrids were collected in aqueous solution of $CaCl_2$ at 1.0 wt% during 40 min (for microgels caracterization and AAS assays) or 60 min (for antimicrobial activity assays) so as to obtain a suspension of microgels equivalent to 200 μL or 300 μL of dispersed phase, respectively. Then microgels were washed by centrifugation (2000 rpm, 5 min) and stored at 4 °C in the $CaCl_2$ solution (1 mL).

2.6. Characterization of calcium-alginate microgels containing nanohybrids

2.6.1. Imaging

The microgels containing CNC, CNC/AgNP and TChiNC/AgNP were analyzed using phase contrast and fluorescence microscopy. Images were captured with an Olympus IX51 inverse microscope (Olympus, France) equipped with phase contrast illumination, a standard UV filter (Exciter filter (BP) 330−385 nm, Dichroic Mirror (DM) 400, Barrier Filter (BA) 420 nm) and a digital camera (Sony, SCD-SX90). Presence of nanocrystals was visualized after addition of 100 μl of calcofluor-white (CW) at 0.01 wt% in 1 mL of suspension of microgels. The size distributions of the microbeads (N = 40) were analyzed using the ImageJ freeware v1.35c.

2.6.2. Atomic absorption spectroscopy for microgels

A similar procedure was used to determine the AgNP content in microgels. A controlled volume of microgels equivalent to 200 μL of dispersed phase was mixed with 10 mL of H_2O/aqua regia mixture for 24 h and then analyzed. For each sample, two independent measurements were performed and the final AgNP content was expressed in mg of AgNP per mL of hybrids suspension.

2.7. Antimicrobial activity

Antimicrobial activities of microgels were assessed against 9 indicator prokaryotic and eukaryotic organisms (Table S1). After precultures in 10 mL of appropriate nutrient broth (Table S1) for 24 h at 30 °C, indicator strains were diluted and inoculated in 96-microplates at an initial concentration of 10^3 CFU/mL approximately, in a total volume

of 200 μL. Each strain was inoculated with 20 μL of microgels suspension or alginate alone. Quantities of alginate, hybrids and silver into microgels suspensions were estimated taking into account the equivalent volume of 300 μL of dispersed phase, composed of 1 wt% of alginate and 0.5 wt% of hybrids, stored in a total volume of 1000 μL of $CaCl_2$ solution. Thereby, each inoculum of microgels suspension was composed of 0.3 mg/mL of alginate and 0.15 mg/mL of hybrids with 1.59 μg/mL or 1.26 μg/mL of silver, respectively for CNC/AgNPs or TChiNC/AgNPs hybrids according to AAS results. Negative controls corresponding to the target strain without microgels were performed in 5 replicates. The impact of microgels on the target growth was estimated by the DO600nm measurement (Varioskan LUX, Thermo Fisher Scientific, France) at 1 h, 4 h, 20 h, 24 h, 48 h and 72 h, at 30 °C.

3. Results and discussion

3.1. Transposition of silver nanohybridization method onto chitin nanocrystals

The first objective of the present study was to enlarge the hybridization method to other bio-based nanocrystals. ChiNCs and TChiNCs were used as new charged substrates for nucleation and growth of AgNP onto their surface and compared to CNCs. These three templates present different surface charge: (i) CNCs are negatively charged after the sulfuric acid hydrolysis inducing sulfate half esters (OSO3−) onto their surface; (ii) ChiNCs are weakly positively charged due to N-acetylglucosamine groups that form primary amino groups available at their surface after partial deacetylation; and (iii) TChiNCs are simultaneously weakly positively and negatively charged after the surface TEMPO-mediated oxidation that substitute some hydroxyl into carboxyl groups onto the surface. It was previously shown on AgNPs grafted on various CNCs that the OH groups served as nucleation point regardless of the surface charge; however, the induced repulsion could better disperse the CNCs leading to higher accessibility to the OH groups (Musino et al., 2020). Results obtained in the present work confirmed this assumption, and the surface-modification of ChiNCs by TEMPO oxidation improved their dispersion in water compared to the untreated samples (i.e., electrostatic repulsion).

The silver precursor ($AgNO_3$) was first dissolved in the CNC, ChiNC or TChiNC aqueous suspensions, and in a second step the chemical reducer ($NaBH_4$) led to the formation of AgNPs. As shown from STEM images (Fig. 1a), AgNPs were grafted and well-dispersed onto CNC, ChiNC, TChiNC surface. Furthermore, the analysis of STEM images allowed to determine the average diameter of AgNPs in the hybrids, which was found equal to 20.4 ± 13 nm, 22.1 ± 14 nm and 24.2 ± 14 nm for the CNC/AgNP, the ChiNC/AgNP and the TChiNC/AgNP system, respectively. The AgNP size distributions are reported in Figure SI1. These results were in accordance with a previous study on hybrids using bacterial CNC that reported a well-dispersed state of CNC/AgNPs, while AgNPs synthetized in the same conditions without CNC rapidly aggregated. This confirmed the positive effect of hybridization on the dispersion and on the size distribution of AgNP, regardless of the CNC, ChiNC or TChiNC source (Musino et al., 2021).

It can be also observed that the AgNPs formation induced a color change of the sample from translucent to yellow; this corresponded to the appearance of a dominant in-plane absorption peak at λ_{max} around 400 nm in the UV-Vis spectra (Fig. 1b) typical of well-dispersed AgNPs and thus corroborating previous result (Musino et al., 2021). The intensity of the UV-Vis peak was quite similar for all the samples showing a similar OH accessibility of the substrates. They were also characterized by a very similar AgNP content, as estimated by AAS in mg AgNP / g of hybrid (i.e., CNC/AgNP at 0.078 ± 0.003 mg/g, ChiNC/AgNP at 0.069 ± 0.003 mg/g, TChiNC/AgNP at 0.075 ± 0.002 mg/g); which corresponds to 7 to 8 wt% of AgNP content for the three hybrids.

The structure of AgNPs in the hybrid suspensions were determined by XRD. As reported in Fig. 1c, the XRD diffractograms proved the presence of AgNPs in a crystalline form through the peak associated to the (111) lattice place of a face-centered cubic silver structure (i.e., $2\theta = 38°$, JCPDS Card No. 89-3722). Other less intense peaks were recorded at angles 44° and 64°, corresponding to (200) and (220) crystalline silver plans, respectively. These results proved the presence of silver onto the nanocrystals.

These results showed the efficiency of Ag^+ hybridization on CNC,

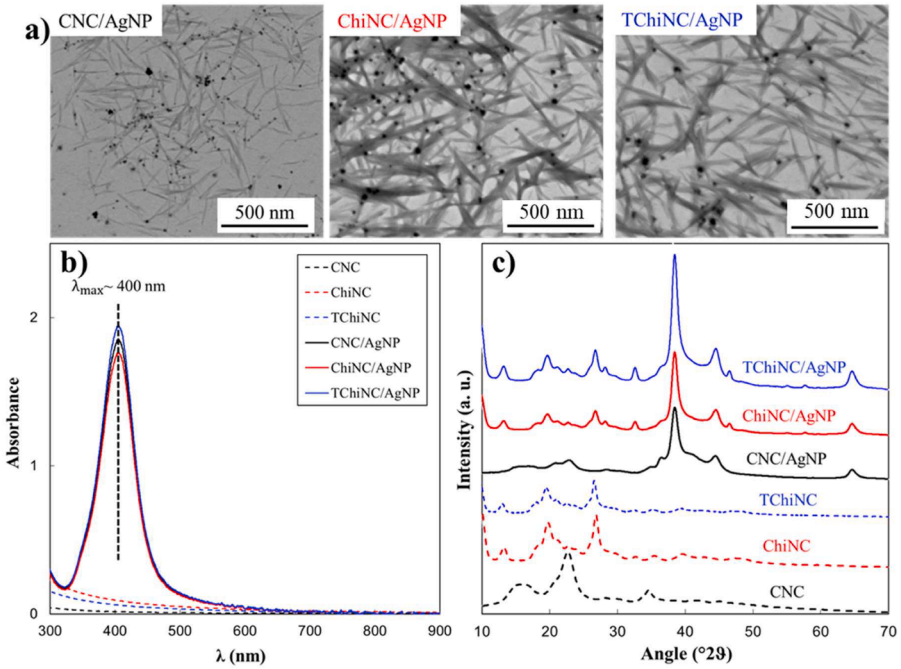

Fig. 1. a) STEM images of AgNPs grafted onto various bio-based support, b) UV-Vis peaks at 400 nm corresponding to AgNP in-plane dipole surface plasmon resonance, and c) XRD diffrectograms of CNC/AgNP, ChiNC/AgNP, TChiNC/AgNP hybrids with characteristic 2θ diffraction peaks (38°, 44° and 64°) of crystalline silver with a lattice plane of face-centered cubic.

ChiNC and TChiNC confirming the high potential of the nanohybrids preparation method whatever the source of nanocrystals. This offers several posibilities for the design of ecological silver nanohybrids with good control of the AgNPs content and size, and highly dispersable in aqueous medium. It is then interesting to consider their encapsulation in a hydrogel that can carry them to the required target. This was carried out only with CNC and TChiNC considering the similar results obtained in dispersion, size and silver content of the nanohybrids with ChiNC and TChiNC.

3.2. Encapsulation of silver nanohybrids into calcium-alginate microgels using a microfluidic device

Encapsulation with biopolymers is an alternative to reduce adverse effects and improve the physicochemical properties of metallic nanoparticles. Therefore, the second objective of the present work was dedicated to developp a microfluidic method leading to the encapsulation of silver nanohybrids without impact of reagents and process on nanohybrids dispersion. Among the various classical gelling agents generally used, alginate was selected due to its availability, biocompatibility, biodegradability and low cost. Its gelation facilities into hydrogel was also a major advantage for a matrix able to retain the hybrids and limit their early relesase. Indeed, as a natural linear polymer composed of blocks of (1,4)-linked β -D-mannuronate (M) and α -L-guluronate (G), with alternating M and G residues, alginate forms a physical hydrogel in the presence of divalent cations, such as calcium, following the egg-box model (Grant et al., 1973). Alginate gelation can be obtained following two different mechanisms: external and internal gelation. Several variations of each mechanisms deployed in microfluidics, and using calcium as ionic source, were described in the literature (Chen et al., 2021). In the case of external gelation, the ionic cross-linking was induced by diffusion of solubilized Ca^{2+} ions from an aqueous solution supplemented with $CaCl_2$, towards the alginate droplets ON- or OFF-chip. The presence of coalescence phenomena before gelation, and deformation of microgels during transit through the oil-water interface, induced variations in the size and shape of migrogels (Oveysi et al., 2023; Sattari et al., 2021), While in the internal mode the gelation occured inside the microfluidic device though the dissolution of water-insoluble $CaCO_3$ under reduce pH control, so as to fix directly the size of alginate microgels (Huang et al., 2021; Paiboon et al., 2023). In the present study, a two-step method was used to generate Ca-alginate microgels containing silver nanohybrids, using internal mode of gelation to fix rapidly the microgels and limit coalescence and deformation phenomena (Marquis et al., 2016). The first step consisted to prepare the dispersed phase containing nanohybrids by gently vortex mixing, to avoid a possible detachment of AgNPs from the nanocrystals (Fig. 2a-1). Brown (CNC/AgNPs) and dark yellow (TChtiNC/AgNPs) colors of mix samples revealed well-dispersed AgNPs in the aqueous solution before being introduced inside the microfluidic device, as it was previously demonstrated during hybrid suspension preparations. The presence of alginate and $CaCO_3$ had no impact on hybrids dispersion (Fig. 2a-2). In the second step, the aqueous suspension was injected in a flow of sunflower oil to generate oil-in-water emulsion through an inherently hydrophobic PDMS microfluidic device (Eddington et al., 2006). At the first FFD junction, aqueous alginate droplets containing nanohybrids and $CaCO_3$ were formed, followed by the initiation of the gelation, by internal mode, at the second junction (Fig. 2b) (Marquis et al., 2012; Zhang et al., 2007). Acetic acid diffused into the aqueous droplets, triggering the release of Ca^{2+} ions from $CaCO_3$ dissolution which cross-linked alginates chains and thus led to the formation of the hydrogel network. The presence of a second junction for the continuous phase avoided cap-formation by early gelation of alginate at the first FFD junction (Marquis et al., 2012). At the end of the process, the Ca-Alginate microgels obtained had a diameter of 46 ± 10 μm and 51 ± 12 μm in the presence of CNC/AgNPs and TChiNC/AgNPs, respectively. Ca-alginate microgels stored for several months (over 12 months) in 1 wt % $CaCl_2$ solution at 4 °C remained stable in size and shape (results not shown). Obtaining hightly stable microgels confirmed the effectiveness of the method without inherent incidents from generation to storage during long period of time.

3.3. The microgel preparation method enabled efficient AgNP encapsulation

Next, the efficient AgNP encapsulation in alginate microgels was demonstrated using calcofluor-white (CW) as fluorescence dye. CW was

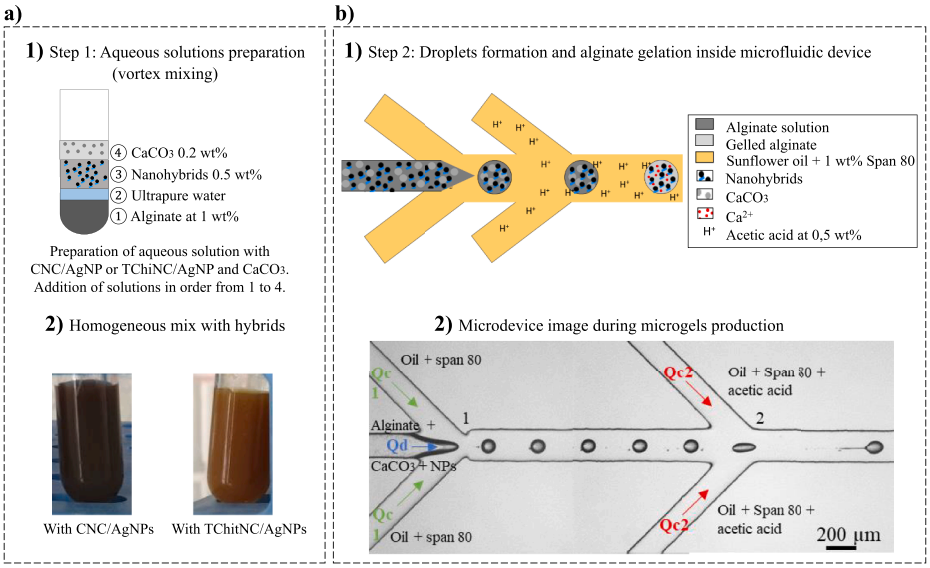

Fig. 2. Schematic representation of the preparation of microhydrogels containing nanohybrids. a-1) Step 1: Aqueous solutions preparation by vortex mixing. Distribution of concentrations for each material of the mixture. a-2) Sample of hybrids with $CaCO_3$ and alginate at optimal concentration conditions with brown (CNC/AgNPs) and dark yellow (ChitNC/AgNPs) colors. b-1) Step 2: Formation of droplets and alginate gelation in the microfluidic device. b-2) Optical microscopy images of microgels production inside the microdevice. Qd: dispersed phase (Alginate + $CaCO_3$ + nanohybrids); Qc1: continuous phase (Sunflower seed oil + Span 80 at 1 wt %); Qc2: continuous phase (Sunflower seed oil + Span 80 at 1 wt% + acetic acid at 0.5 wt%). The flow rates of the alginate solutions and oil in each channel were Qd = 5 μl/min, Qc1 and Qc2 = 90 μL/min.

selected due to its binding facilities to β(1–3) and β(1–4) oriented structural polysaccharides such as crystalline cellulose and chitin. CW fluoresces with an intense bluish/white color when excited with ultraviolet, allowing hybrids localization (Harrington & Hageage, 2003). Previously, a negative control confirmed that CW did not bind alginate and $CaCO_3$. Indeed, no fluorescence was observed in NPs-free Ca-alginate microgels (Fig. 3a). On the other hand, a positive control, done on Ca-alginate microgels containing CNC but no AgNP, showed a homogeneous bluish/white color due to cellulose without diffusion outside the microgels (Fig. 3b). These control samples validated the CW-labeling method to demonstrate the effective encapsulation of biobased nanoparticles. Similarly to the AgNP-free nanocrystal sample, the CW-labeling showed a homogeneous bluish/white color in microgels containing either CNC/AgNP (Figue 3c) or TChiNC/AgNP (Figue 3d), and no diffusion outside the microgels was observed.

The amount of silver into the microgels was also analysed by AAS investigations to measue the concentration in AgNP in mg per ml of microgel. Content of 0.053 mg AgNP/mL (i.e. 5.3 wt%) and 0.042 mg AgNP/mL (i.e. 4.2 wt%) of silver were measured in CNC/AgNP and TChiNC/AgNP microgels, respectively.

All these results demonstrated the efficient encapsualtion, into microgels, of Ag^+ through hybridization with biobased nanocrystals. They confirmed the presence of silver into microgels very well dispersed, as no aggregation was observed, and at concentration above the minimum inhibitory concentration (MIC) of AgNP determined at 0.016 mg AgNP/ml of hybrid (i.e. 1.6 wt%) in previous work (Musino et al., 2021). Moreover, the hybridization of Ag^+ on solid nanocrystals, as nanocomposites, reduced their release and could avoid the cytotoxic effect of free Ag^+ on human cells while maintaining antibacterial capability (Liu & Man, 2017; Marchioni et al., 2020). All these data demonstrate a potential safe use of these types of smart biomaterials for biomedical applications.

3.4. *Screening of antimicrobial activity of silver hybrids encapsulated into alginate microgels*

To demonstrate the feasibility of bio-sourced silver immobilization systems, an antimicrobial activity analysis was managed to identify sensitive species to low silver contents. Antimicrobial activities of microgels were assessed against 9 indicator strains representing microbial diversity in term of organism (prokaryotic and eukaryotic cells), cell-wall structure (Gram positive and Gram negative bacteria) and involved in human infections, fish diseases and food spoilage (Table S1). The impact of the presence of microgels, or sample controls of alginate solution, on the indicator strain growth was assessed by absorbance measurement for 72 h, using miniaturized methods. Fig. 4 compared the concentration of indicator strains at their stationary phase in the different conditions. Alginate alone did not affect the growth of targets, the observed modifications on growth were thus related to the encapsulated nanohybrids. Previous study showed that a lowest AgNP content

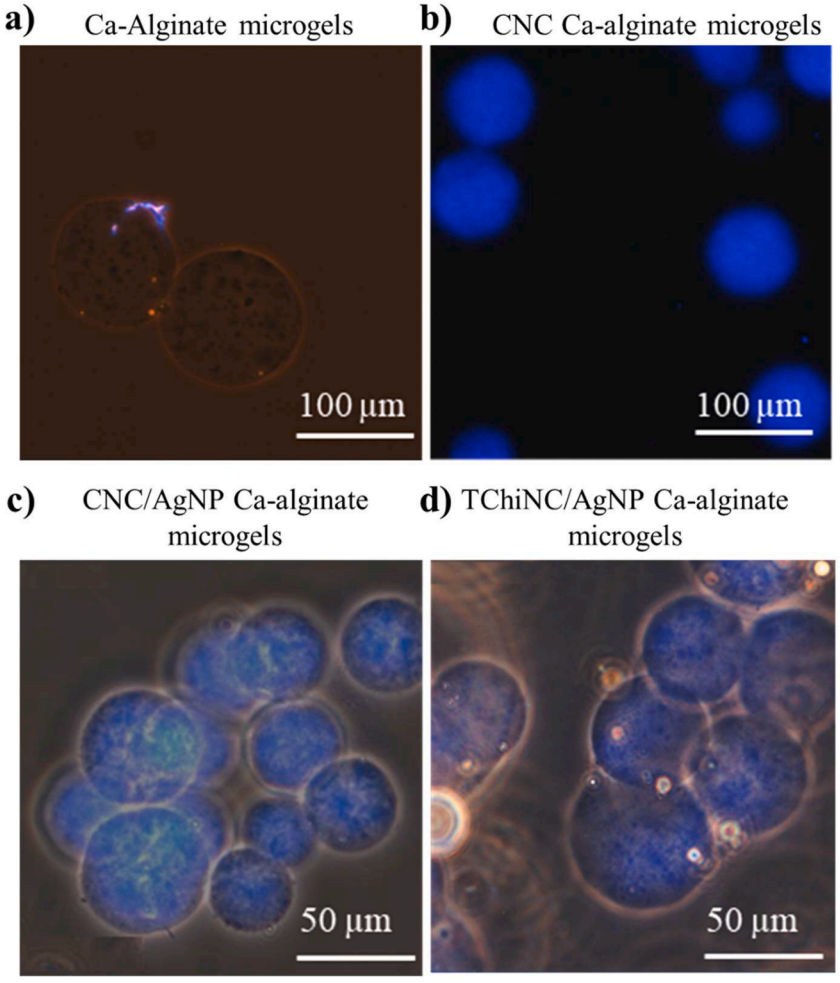

Fig. 3. Phase contrast microscopy observations in Ultra Violet of the Ca-alginate microgels staining the nanocrystals with calcofluor-white (0.009 g/L). Upwards are control samples with a) no labeling in pure Ca-alginate microgels and b) effective labeling in microgels containing CNC showing no passive diffusion of nanocrystals in time (same results were obtained with ChiNC). Downwards are samples of Ca-alginate microgels with effective encapsulation of nanohybrids whitout passive diffusion for c) CNC/AgNP: 46 ± 10 µm in diameter, and d) TChiNC/AgNP: 51 ± 12 µm in diameter.

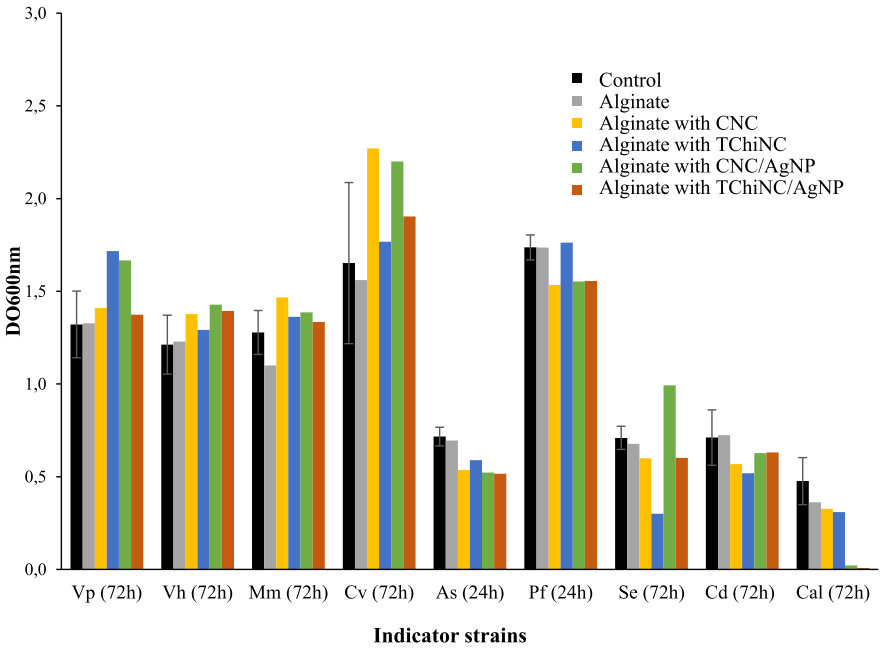

Fig. 4. Comparison of indicator strain concentrations at the stationary phase, in the presence and absence of the four different microgels with 0.15 mg/ml of hybrids or 0.3 mg/ml of alginate. The control corresponded to the growth of the indicator strain without microgel. It was performed in five replicates for each indicator strain. The incubation time, considered as the stationary phase for the bacterial strain, was indicated in brackets. Indicator strains: *Vibrio parahaemolyticus* LMG 2850 (Vp), *Vibrio harveyi* LMG 4044 (Vh), *Morganella morganii* CIP A231T (Mm), *Chromobacterium violaceum* CIP 103350^{T} (Cv), *Aeromonas salmonicida* CIP 103209^{T} (As), *Pseudomonas fluorescens* CIP 69.13^{T} (Pf), *Carnobacterium divergens* V41 (Cd), *Staphylococcus epidermidis* CIP 68.21 (Se), *Candida albicans* DSM 1386 (Cal).

of 0.048 μg led to a well-detectable antimicrobial effect after disk-diffusion on agar plate (Musino et al., 2021). In the present work, microgels containing AgNPs showed only a little effect on bacterial growth, which could be explained by the lower contents of silver after inoculation, which were of 0.032 μg and 0.025 μg in solution per well for CNC/AgNPs and TChiNC/AgNPs, respectively. Interestingly, an inhibitory activity on the fungi responsible for candidiasis, *Candida albicans,* was observed at these low contents of silver (Figs. 4, 5). Candidiasis is considered a major health problem, particularly for their ability to produce biofilms and virulence factors and to develop antifungal resistances (Henriques & Williams, 2020; Mayer et al., 2013; Tsui et al., 2016), new therapies and microcarriers are needed. A weak inhibition of this indicator strain was observed in absence of AgNP (Alginate with CNC and TChiNC) confirming the safety of native NPs. Both microgels containing AgNPs (Alginate with CNC/AgNPs and TChiNC/AgNPs) maintained a low concentration of *C. albicans* DSM1386 while 72 h, and allowed finally a reduction at least by five the *C. albicans* concentration (Fig. 5). These preliminary results are consistent with the inhibitory activities of silver complexed with various ligands against *C. albicans* previously described, such as the reduction of up to 80 % of the *Candida* filamentous forms (corresponding to the pathogen form) with Ag-natural NP (Gómez-Garzón et al., 2021b) or the growth inhibition of Ag-NHC (N-heterocyclic carbenes) (Dileepan et al., 2021).

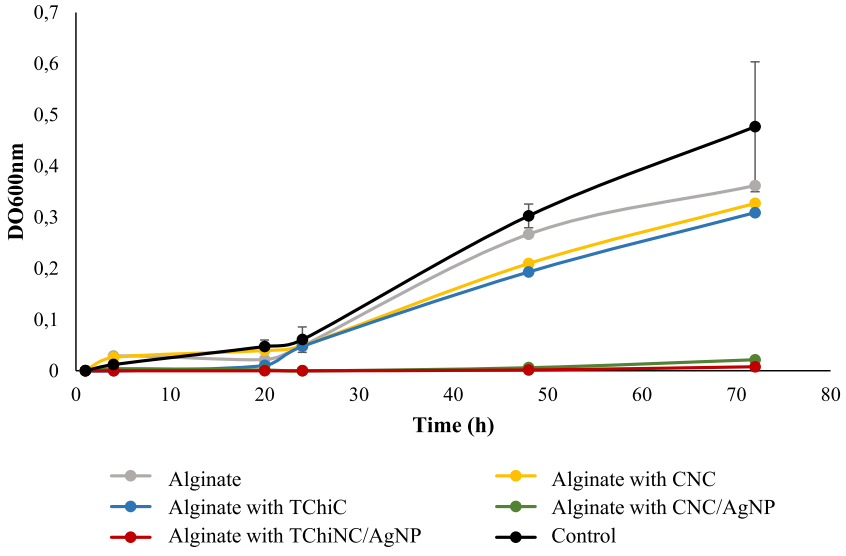

Fig. 5. *Candida albicans* DSM 1386 kinetic growth in presence of microgels with 0.15 mg/ml of hybrids or 0.3 mg/ml of alginate, in Luria-Bertani (LB) medium at 30 °C. The culture of *Candida albicans* in LB medium, used as control, was performed in five replicates.

4. Conclusion

This study demonstrated the design of ecological silver nanohybrids based on biosourced nanocrystals from chitin (ChiNC or TChiNC). A comparative study, including nanocrystals from cellulose (CNC), showed, on STEM images, individual AgNPs with a size of 22 nm, regardless of the nature and charge of the substrate, which confirms the versatility of the developped method. It resulted in bioparticles perfectly dispersible in water, bearing 7–8 wt.% of AgNPs grafted onto their surface. For more controlled applications, the hybrids were encapsulated into calcium-alginate microgels using microfluidic tools. It allowed a double level of immobilization of AgNPs offering very stable carriers of 45–50 μm in diameter with a precise control of the silver concentration. It led to a high potential controlled release system for silver with no passive diffusion outside the microgels.

The preliminary assays to assess the potential antimicrobial activities of these low-silver content microgels have shown a significant inhibitory effect on *Candida albicans*. Results obtained in the present work offer a promising bio-friendly approach based on the controlled release of silver that will find a wide range of applications in the pharmaceutical, cosmetics and plant science.

Supporting Information

AgNP size distributions; Microchannel dimensions of the microfluidic device; Indicator strain characteristics used for antimicrobial activity.

CRediT authorship contribution statement

Mélanie Marquis: Investigation, Methodology, Writing – original draft, Writing – review & editing. **Dafne Musino:** Conceptualization, Investigation, Methodology, Writing – original draft. **Valentin Gemin:** Investigation. **Laetitia Kolypczuk:** Investigation. **Delphine Passerini:** Investigation, Methodology, Writing – original draft, Writing – review & editing. **Isabelle Capron:** Conceptualization, Supervision, Writing – review & editing.

Declaration of Competing Interest

The authors declare that they have no known competing financial interests or personal relationships that could have appeared to influence the work reported in this paper.

Data availability

Data will be made available on request.

Acknowledgments

We gratefully acknowledge F. X. Lefevre and N. Guichard (Université de Nantes) for support in AAS experiments, B. Pontoire (BIA-Nantes) for performing XRD acquisitions, B. Novales for helping in acquisition of STEM images. This work is a contribution to the Labex SERENADE (n° ANR-11-LABX-0064) funded by the French government program, "Investissement d'Avenir", of the French National Research Agency (ANR) through the A*MIDEX project (n° ANR-11-IDEX-0001-02). Our work was initiated in the context of the French research group dedicated to sustainable materials (GDR DUMBIO).

Supplementary materials

Supplementary material associated with this article can be found, in the online version, at doi:10.1016/j.carpta.2023.100405.

References

Aisida, S. O., Akpa, P. A., Ahmad, I., Zhao, T., Maaza, M., & Ezema, F. I. (2020). Bio-inspired encapsulation and functionalization of iron oxide nanoparticles for biomedical applications. *European Polymer Journal, 122*, Article 109371. https://doi.org/10.1016/j.eurpolymj.2019.109371

Araki, J., & Hida, Y. (2018). Comparison of methods for quantitative determination of silver content in cellulose nanowhisker/silver nanoparticle hybrids. *Cellulose (London, England), 25*(2), 1065–1076. https://doi.org/10.1007/s10570-017-1640-z

Bashir, S., Ali, A., Bashir, M., Aftab, A., Ghani, T., Javed, A., Rafique, S., Shah, A., Casadevall i Solvas, X., & Inayat, M. H. (2022). Droplet-based microfluidic synthesis of silver nanoparticles stabilized by PVA and PVP: Applications in anticancer and antimicrobial activities. *Chemical Papers, 76*(11), 7205–7216. https://doi.org/10.1007/s11696-022-02403-w

Cai, L., Huang, Y., Duan, Y., Liu, Q., Xu, Q., Jia, J., Wang, J., Tong, Q., Luo, P., Wen, Y., Peng, L., Wu, Q., Hang, X., Jiang, H., Zhu, P., Yang, Y., Zhou, B., Zeng, L., Bi, H., & Chen, J. (2021). Schiff-base silver nanocomplexes formation on natural biopolymer coated mesoporous silica contributed to the improved curative effect on infectious microbes. *Nano Research, 14*(8), 2735–2748. https://doi.org/10.1007/s12274-020-3279-6

Chen, M., Bolognesi, G., & Vladisavljević, G. T. (2021). Crosslinking strategies for the microfluidic production of microgels. *Molecules (Basel, Switzerland), 26*(12), 3752. https://doi.org/10.3390/molecules26123752

Cinel, V. D. P., Taketa, T. B., de Carvalho, B. G., de la Torre, L. G., de Mello, L. R., da Silva, E. R., & Han, S. W. (2021). Microfluidic encapsulation of nanoparticles in alginate microgels gelled via competitive ligand exchange crosslinking. *Biopolymers*, (7), 112. https://doi.org/10.1002/bip.23432

Dakal, T. C., Kumar, A., Majumdar, R. S., & Yadav, V. (2016). Mechanistic basis of antimicrobial actions of silver nanoparticles. *Frontiers in Microbiology, 7*. https://doi.org/10.3389/fmicb.2016.01831

Dang, Q., Liu, C., Wang, Y., Yan, J., Wan, H., & Fan, B. (2016). Characterization and biocompatibility of injectable microspheres-loaded hydrogel for methotrexate delivery. *Carbohydrate Polymers, 136*, 516–526. https://doi.org/10.1016/j.carbpol.2015.09.084

Dileepan, A. G. B., Ganeshkumar, A., Ranjith, R., Maruthamuthu, D., Rajaram, R., & Rajam, S. (2021). Killing effects of Candida albicans through alteration of cellular morphology and growth metabolism using Tris-NHC ligand coordinated to AgI and CuI. *Journal of Molecular Structure, 1225*, Article 129117. https://doi.org/10.1016/j.molstruc.2020.129117

Eddington, D. T., Puccinelli, J. P., & Beebe, D. J. (2006). Thermal aging and reduced hydrophobic recovery of polydimethylsiloxane. *Sensors and Actuators B: Chemical, 114*(1), 170–172. https://doi.org/10.1016/j.snb.2005.04.037

Ernest Ravindran, R. S., Subha, V., & Ilangovan, R. (2020). Silver nanoparticles blended PEG/PVA nanocomposites synthesis and characterization for food packaging. *Arabian Journal of Chemistry, 13*(7), 6056–6060. https://doi.org/10.1016/j.arabjc.2020.05.005

Ferashteh, Nejaddehbashi, Mahmoud, Hashemitabar, Vahid, Bayati, Eskandar, Moghimipour, Jabraeel, Movaffagh, Mamoud, Orazizadeh, & Mahammadreza, Abbaspour (2019). Incorporation of silver sulfadiazine into an electrospun composite of polycaprolactone as an antibacterial scaffold for wound healing in rats. *Cell Journal, 21*(4), 379–390.

Gómez-Garzón, M., Gutiérrez-Castañeda, L. D., Gil, C., Escobar, C. H., Rozo, A. P., González, M. E., & Sierra, E.v. (2021a). Inhibition of the filamentation of Candida albicans by Borojoa patinoi silver nanoparticles. *SN Applied Sciences, 3*(2), 195. https://doi.org/10.1007/s42452-020-04103-0

Gómez-Garzón, M., Gutiérrez-Castañeda, L. D., Gil, C., Escobar, C. H., Rozo, A. P., González, M. E., & Sierra, E.v. (2021b). Inhibition of the filamentation of Candida albicans by Borojoa patinoi silver nanoparticles. *SN Applied Sciences, 3*(2), 195. https://doi.org/10.1007/s42452-020-04103-0

Grant, G. T., Morris, E. R., Rees, D. A., Smith, P. J. C., & Thom, D. (1973). Biological interactions between polysaccharides and divalent cations: The egg-box model. *FEBS Letters, 32*(1), 195–198. https://doi.org/10.1016/0014-5793(73)80770-7

Harrington, B. J., & Hageage, G. J. (2003). Calcofluor white: A review of its uses and applications in clinical mycology and parasitology. *Laboratory Medicine, 34*(5), 361–367. https://doi.org/10.1309/EPH2TDT8335GH0R3

Hendiger, E. B., Padzik, M., Sifaoui, I., Reyes-Batlle, M., López-Arencibia, A., Rizo-Liendo, A., Bethencourt-Estrella, C. J., San Nicolás-Hernández, D., Chiboub, O., Rodríguez-Expósito, R. L., Grodzik, M., Pietruczuk-Padzik, A., Stępień, K., Olędzka, G., Chomicz, L., Piñero, J. E., & Lorenzo-Morales, J. (2020). Silver nanoparticles as a novel potential preventive agent against acanthamoeba keratitis. *Pathogens (Basel, Switzerland), 9*(5), 350. https://doi.org/10.3390/pathogens9050350

Henriques, M., & Williams, D. (2020). Pathogenesis and virulence of *Candida albicans* and *Candida glabrata*. *Pathogens (Basel, Switzerland), 9*(9), 752. https://doi.org/10.3390/pathogens9090752

Huang, L., Wu, K., He, X., Yang, Z., & Ji, H. (2021). One-Step microfluidic synthesis of spherical and bullet-like alginate microcapsules with a core–shell structure. *Colloids and Surfaces A: Physicochemical and Engineering Aspects, 608*, Article 125612. https://doi.org/10.1016/j.colsurfa.2020.125612

Huang, L., Yu, L., Yin, X., Lin, Y., Xu, Y., & Niu, Y. (2022). Silver nanoparticles with vanadium oxide nanowires loaded into electrospun dressings for efficient healing of bacterium-infected wounds. *Journal of Colloid and Interface Science, 622*, 117–125. https://doi.org/10.1016/j.jcis.2022.04.026

Jiménez-Saelices, C., Trongsatitkul, T., Lourdin, D., & Capron, I. (2020). Chitin pickering emulsion for oil inclusion in composite films. *Carbohydrate Polymers, 242*, Article 116366. https://doi.org/10.1016/j.carbpol.2020.116366

Klemm, D., Kramer, F., Moritz, S., Lindström, T., Ankerfors, M., Gray, D., & Dorris, A. (2011). Nanocelluloses: A new family of nature-based materials. *Angewandte Chemie International Edition, 50*(24), 5438–5466. https://doi.org/10.1002/anie.201001273

Leawhiran, N., Pavasant, P., Soontornvipart, K., & Supaphol, P. (2014). Gamma irradiation synthesis and characterization of AgNP/gelatin/PVA hydrogels for antibacterial wound dressings. *Journal of Applied Polymer Science, 131*(23). https://doi.org/10.1002/app.41138. n/a-n/a.

Liu, X., & Man, H. C. (2017). Laser fabrication of Ag-HA nanocomposites on Ti6Al4V implant for enhancing bioactivity and antibacterial capability. *Materials Science and Engineering: C, 70*, 1–8. https://doi.org/10.1016/j.msec.2016.08.059

Mancini, M., Moresi, M., & Rancini, R. (1999). Mechanical properties of alginate gels: Empirical characterisation. *Journal of Food Engineering, 39*(4), 369–378. https://doi.org/10.1016/S0260-8774(99)00022-9

Marchioni, M., Veronesi, G., Worms, I., Ling, W. L., Gallon, T., Leonard, D., Gateau, C., Chevallet, M., Jouneau, P.-H., Carlini, L., Battocchio, C., Delangle, P., Michaud-Soret, I., & Deniaud, A. (2020). Safer-by-design biocides made of tri-thiol bridged silver nanoparticle assemblies. *Nanoscale Horizons, 5*(3), 507–513. https://doi.org/10.1039/C9NH00286C

Markert, C. D., Guo, X., Skardal, A., Wang, Z., Bharadwaj, S., Zhang, Y., Bonin, K., & Guthold, M. (2013). Characterizing the micro-scale elastic modulus of hydrogels for use in regenerative medicine. *Journal of the Mechanical Behavior of Biomedical Materials, 27*, 115–127. https://doi.org/10.1016/j.jmbbm.2013.07.008

Marquis, M., Alix, V., Capron, I., Cuenot, S., & Zykwinska, A. (2016). Microfluidic encapsulation of pickering oil microdroplets into alginate microgels for lipophilic compound delivery. *ACS Biomaterials Science & Engineering, 2*(4), 535–543. https://doi.org/10.1021/acsbiomaterials.5b00522

Marquis, M., Davy, J., Fang, A., & Renard, D. (2014). Microfluidics-assisted diffusion self-assembly: toward the control of the shape and size of pectin hydrogel microparticles. *Biomacromolecules, 15*(5), 1568–1578. https://doi.org/10.1021/bm401596m

Marquis, M., Renard, D., & Cathala, B. (2012). Microfluidic generation and selective degradation of biopolymer-based Janus microbeads. *Biomacromolecules, 13*(4), 1197–1203. https://doi.org/10.1021/bm300159u

Matalanis, A., Jones, O. G., & McClements, D. J. (2011). Structured biopolymer-based delivery systems for encapsulation, protection, and release of lipophilic compounds. *Food Hydrocolloids, 25*(8), 1865–1880. https://doi.org/10.1016/j.foodhyd.2011.04.014

Mayer, F. L., Wilson, D., & Hube, B. (2013). Candida albicans pathogenicity mechanisms. *Virulence, 4*(2), 119–128. https://doi.org/10.4161/viru.22913

Monerris, M., Broglia, M., Yslas, I., Barbero, C., & Rivarola, C. (2017). Antibacterial polymeric nanocomposites synthesized by in-situ photoreduction of silver ions without additives inside biocompatible hydrogel matrices based on N-isopropylacrylamide and derivatives. *Express Polymer Letters, 11*(12), 946–962. https://doi.org/10.3144/expresspolymlett.2017.91

Muñoz-Bonilla, A., Echeverria, C., Sonseca, Á., Arrieta, M. P., & Fernández-García, M. (2019). Bio-based polymers with antimicrobial properties towards sustainable development. *Materials, 12*(4), 641. https://doi.org/10.3390/ma12040641

Musino, D., Devcic, J., Lelong, C., Luche, S., Rivard, C., Dalzon, B., Landrot, G., Rabilloud, T., & Capron, I. (2021a). Impact of physico-chemical properties of cellulose nanocrystal/silver nanoparticle hybrid suspensions on their biocidal and toxicological effects. *Nanomaterials, 11*(7), 1862. https://doi.org/10.3390/nano11071862

Musino, D., Rivard, C., Landrot, G., Novales, B., Rabilloud, T., & Capron, I. (2021b). Hydroxyl groups on cellulose nanocrystal surfaces form nucleation points for silver nanoparticles of varying shapes and sizes. *Journal of Colloid and Interface Science, 584*, 360–371. https://doi.org/10.1016/j.jcis.2020.09.082

Musino, D., Rivard, C., Novales, B., Landrot, G., & Capron, I. (2020). Tuning of Ag nanoparticle properties in cellulose nanocrystals/ag nanoparticle hybrid suspensions by H2O2 redox post-treatment: The role of the H2O2/AgNP ratio. *Nanomaterials, 10*(8), 1559. https://doi.org/10.3390/nano10081559

Neves, A. C. O., Viana, A. D., Menezes, F. G., Wanderlei Neto, A. O., Melo, M. C. N., & Gasparotto, L. H. S. (2021). Biospectroscopy and chemometrics as an analytical tool for comparing the antibacterial mechanism of silver nanoparticles with popular antibiotics against Escherichia coli. *Spectrochimica Acta Part A: Molecular and Biomolecular Spectroscopy, 253*, Article 119558. https://doi.org/10.1016/j.saa.2021.119558

Nikolov, A. S., Stankova, N. E., Karashanova, D. B., Nedyalkov, N. N., Pavlov, E. L., Koev, K. Tz., Najdenski, Hr., Kussovski, V., Avramov, L. A., Ristoscu, C., Badiceanu, M., & Mihailescu, I. N (2021). Synergistic effect in a two-phase laser procedure for production of silver nanoparticles colloids applicable in ophthalmology. *Optics & Laser Technology, 138*, Article 106850. https://doi.org/10.1016/j.optlastec.2020.106850

Ou, Q., Huang, K., Fu, C., Huang, C., Fang, Y., Gu, Z., Wu, J., & Wang, Y. (2020). Nanosilver-incorporated halloysite nanotubes/gelatin methacrylate hybrid hydrogel with osteoimmunomodulatory and antibacterial activity for bone regeneration. *Chemical Engineering Journal, 382*, Article 123019. https://doi.org/10.1016/j.cej.2019.123019

Oveysi, M., Zaker, M. A., Peregrino, G., Bazargan, V., & Marengo, M. (2023). Droplet-based fabrication of alginate hydrogel microparticles in presence of surfactants. *Microfluidics and Nanofluidics, 27*(7), 45. https://doi.org/10.1007/s10404-023-02655-2

Paiboon, N., Surassmo, S., Rungsardthong Ruktanonchai, U., Kappl, M., & Soottitantawat, A. (2023). Internal gelation of alginate microparticle prepared by emulsification and microfluidic method: Effect of Ca-EDTA as a calcium source. *Food Hydrocolloids, 141*, Article 108712. https://doi.org/10.1016/j.foodhyd.2023.108712

Perrin, E., Bizot, H., Cathala, B., & Capron, I. (2014). Chitin nanocrystals for pickering high internal phase emulsions. *Biomacromolecules, 15*(10), 3766–3771. https://doi.org/10.1021/bm5010417

Rahman, K., Khan, S. U., Fahad, S., Chang, M. X., Abbas, A., Khan, W. U., Rahman, L., Haq, Z. U., Nabi, G., & Khan, D. (2019). Nano-biotechnology: A new approach to treat and prevent malaria. *International Journal of Nanomedicine, 14*, 1401–1410. https://doi.org/10.2147/IJN.S190692

Reid, M. S., Villalobos, M., & Cranston, E. D. (2017). Benchmarking Cellulose Nanocrystals: From the Laboratory to Industrial Production. *Langmuir, 33*(7), 1583–1598. https://doi.org/10.1021/acs.langmuir.6b03765

Rojas, M. A., Amalraj, J., & Santos, L. S. (2023). Biopolymer-based composite hydrogels embedding small silver nanoparticles for advanced antimicrobial applications: experimental and theoretical insights. *Polymers, 15*(16), 3370. https://doi.org/10.3390/polym15163370

Sattari, A., Janfaza, S., Mashhadi Keshtiban, M., Tasnim, N., Hanafizadeh, P., & Hoorfar, M. (2021). Microfluidic on-chip production of alginate hydrogels using double coflow geometry. *ACS Omega, 6*(40), 25964–25971. https://doi.org/10.1021/acsomega.1c02728

Seidi, F., Khodadadi Yazdi, M., Jouyandeh, M., Dominic, M., Naeim, H., Nezhad, M. N., Bagheri, B., Habibzadeh, S., Zarrintaj, P., Saeb, M. R., & Mozafari, M. (2021). Chitosan-based blends for biomedical applications. *International Journal of Biological Macromolecules, 183*, 1818–1850. https://doi.org/10.1016/j.ijbiomac.2021.05.003

Shoueir, K. R., El-Desouky, N., Rashad, M. M., Ahmed, M. K., Janowska, I., & El-Kemary, M. (2021). Chitosan based-nanoparticles and nanocapsules: Overview, physicochemical features, applications of a nanofibrous scaffold, and bioprinting. *International Journal of Biological Macromolecules, 167*, 1176–1197. https://doi.org/10.1016/j.ijbiomac.2020.11.072

Thiruvengadam, Sriram, & Pandidurai, V. (2014). Synthesis of silver nanoparticles from leaf extract of psidium guajava and its antibacterial activity against pathogens. *International Journal of Current Microbiology and Applied Sciences, 3*(3), 146–152.

Tsui, C., Kong, E. F., & Jabra-Rizk, M. A. (2016). Pathogenesis of *Candida albicans* biofilm. *Pathogens and Disease, 74*(4). https://doi.org/10.1093/femspd/ftw018. ftw018.

Ullah, A. K. M. A., Kabir, M. F., Akter, M., Tamanna, A. N., Hossain, A., Tareq, A. R. M., Khan, M. N. I., Kibria, A. K. M. F., Kurasaki, M., & Rahman, M. M. (2018). Green synthesis of bio-molecule encapsulated magnetic silver nanoparticles and their antibacterial activity. *RSC Advances, 8*(65), 37176–37183. https://doi.org/10.1039/C8RA06908E

Williams, D. F. (2009). On the nature of biomaterials. *Biomaterials, 30*(30), 5897–5909. https://doi.org/10.1016/j.biomaterials.2009.07.027

Yang, C.-H., Wang, L.-S., Chen, S.-Y., Huang, M.-C., Li, Y.-H., Lin, Y.-C., Chen, P.-F., Shaw, J.-F., & Huang, K.-S. (2016). Microfluidic assisted synthesis of silver nanoparticle–chitosan composite microparticles for antibacterial applications. *International Journal of Pharmaceutics, 510*(2), 493–500. https://doi.org/10.1016/j.ijpharm.2016.01.010

Zhang, H., Tumarkin, E., Sullan, R. M. A., Walker, G. C., & Kumacheva, E. (2007). Exploring microfluidic routes to microgels of biological polymers. *Macromolecular Rapid Communications, 28*(5), 527–538. https://doi.org/10.1002/marc.200600776

Zhou, Z., Lu, C., Wu, X., & Zhang, X. (2013). Cellulose nanocrystals as a novel support for CuO nanoparticles catalysts: Facile synthesis and their application to 4-nitrophenol reduction. *RSC Advances, 3*(48), 26066. https://doi.org/10.1039/c3ra43006e